High temperature compressive creep of dense and porous Cr_2AlC in air

Wakako Araki[a,*], Jesus Gonzalez-Julian[b], and Jürgen Malzbender[b]

[a] Department of Mechanical Engineering, Saitama University, Japan; email: araki@mech.saitama-u.ac.jp

[b] Institute of Energy and Climate Research, Forschungszentrum Jülich GmbH

* Corresponding author. araki@mech.saitama-u.ac.jp (W. Araki)

ABSTRACT

The creep behaviours of the dense and porous Cr_2AlC ceramics were investigated, being the first study on creep behaviour of not only Cr_2AlC but also porous MAX phase. The creep rate of the porous Cr_2AlC measured during cooling was significantly lower than the one during heating due to oxide and carbide scales formed during the creep tests at the high temperatures, whilst the dense Cr_2AlC possesses consistent creep rates during heating and cooling. The formation of these scales led to the reinforcement of the porous ceramics and some healing of defects, which significantly improved the creep resistance. A comparison with other porous alloys and ceramics revealed that the oxidised porous Cr_2AlC has a high potential as a refractory material, especially considering its machinability and light-weight.

Keywords: MAX phases; Cr_2AlC; Creep; Porous materials; Oxidation.

1. Introduction

MAX phases are layered materials with a general formula of $M_{n+1}AX_n$, where M is an early transition metal, A is an A-group element of the periodic table, X corresponds to C and/or N, and *n* is typically 1, 2, or 3 [1]. They have attracted a strong interest, in particular in the last years, due to their unique combination of properties, bridging the gap between metals and ceramics [2]. In fact, nowadays, more than 60 different MAX phases have been discovered (this number increases every year), but those MAX phases that contain aluminium as "A" element are of particular interesting for high temperature applications, since these Al-based MAX phases form under oxidizing atmosphere at high temperature, typically > 1000 °C, an external, well-adhered and dense α-Al_2O_3 layer that protects the material against further oxidation [3][4]. This in-situ formation of a protective scale is associated with a volumetric expansion, so that these MAX phases exhibit in addition a self-healing capability [5].

Among all the Al-based MAX phases, Ti_2AlC, Ti_3AlC_2, and Cr_2AlC appear to exhibit the best oxidation and corrosion resistances [3]. As a result, these MAX phases are excellent candidates to be operated at high temperature under aggressive environments due to the above response and the combination of other characteristic features of MAX phases, such as being lightweight, possessing high elastic modulus, thermal and electrical conductivity, being ease machinability with also excellent thermal shock resistance and damage tolerance [6][7][8].

These properties have triggered the development of different structures on the basis of these materials, such as bulk compounds, thin films [9], Ceramic Matrix Composites [10], coatings [11] and porous substrates [12]. These structures have been studied to a greater or lesser extent, but surprisingly, porous MAX phases have only been investigated to a minor extent considering their high potential, i.e. in the form of ceramic foams in applications such as supports for catalytic reactions and membranes, filters for gases, liquids, molten metals or solid particles, and heat exchangers [13]. In fact, the main drawbacks of these reticular ceramic structures – high brittleness, hard machining, complex joining with metals, and high coefficient of thermal expansion (CTE) mismatch – can be overcome by using MAX phase foams. As mentioned, the number of works is limited, and they are mainly focused on the processing routes by sacrificial template [14][15][16][17], replica method [18][19][20] and direct foaming [21][22]. The different routes lead to tailor diverse final microstructures with differences in such as content and size or the porosity, interconnectivity between pores, and thickness of the struts. Regarding the MAX compounds, in these

studies mostly Ti_2AlC and Ti_3AlC_2 have been processed. The reason might be related with the excellent high temperature properties reported for their dense counterparts, and the availability of commercial powders. However, recently results regarding Cr_2AlC porous structures produced by sacrificial template and replica method have been published [20][17].

Unfortunately, publications regarding mechanical characterization results of the developed MAX phase foams appear to be even more limited than the studies on processing, despite their apparent high potential. Elastic modulus and compressive strength at room temperature, as well as thermal conductivity [22], have been evaluated as a function of the porosity [15]. Reticulated MAX phase structures revealed a fully reversible and closed deformation hysteresis loops under subsequent cycles of compression [12]. It was suggested that this implies that the porous material dissipates more energy on an absolute scale than its fully dense counterpart. Therefore, the mechanical response of MAX phase foams is encouraging but more studies are warranted, particularly regarding their elevated temperature behaviour, although an improvement of the compressive strength has been reported after the oxidation at 1200 °C in air for Cr_2AlC foams [17]. The mechanisms are still unclear, but certainly it has to be considered that the in-situ oxide scale formed at high temperature plays a determinant role. The oxide scale, α-Al_2O_3, appeared to be well-adhered and covers seamlessly the whole external surface of the pores, even when they present sharp angles and tight corners [17]. Furthermore, it is important to mention again the self-healing capability of dense Al-based MAX phases, an effect that might be magnified in porous structures due to the larger surface area.

The aim of the current work is to study the effect of the porosity on the creep deformation behaviour of Cr_2AlC material at high temperatures. Cr_2AlC ceramics containing 2, 53 and 73 vol.% porosity were consolidated and tested mostly in air at temperatures up to 1473 K. Effects of porosity, atmosphere, formation of oxide scale and self-healing capability are analysed and discussed in detail, partly aided by complementary microstructural analysis.

2. Experimental

Processing of almost dense and porous Cr_2AlC ceramics was carried out in two consecutives steps. First, Cr_2AlC powder was synthesized from its elemental constituents by liquid/solid state reaction, followed by a

second step to consolidate the ceramics – dense or porous – at high temperature. This process is described in detail elsewhere [23][17]. Briefly, Cr, Al, and C powders (all from Alfa Aesar, Germany) were mixed in a molar ratio of 2:1.1:1, respectively, and uniaxially pressed at 100 MPa. Pellets were heated at 1673 K in argon atmosphere for 3 h to synthesize the Cr_2AlC phase. Then, Cr_2AlC ceramics were ground and milled to obtain the final powder with a unimodal particle size distribution and a mean particle size of 9 µm. Porous ceramics were produced by a sacrificial template method, using ammonium hydrogen bicarbonate (NH_4HCO_3) as temporary space holder material. Cr_2AlC powder was mixed with 60 vol.% and 80 vol.% of NH_4HCO_3, followed by cold uniaxial pressing to obtain pellets of 13 mm diameter and 10 mm height. The space holders were burned-out at low temperature (353 K) in air, and the porous structures were consolidated at 1523 K for 5 h in argon atmosphere. The consolidated porous ceramics present a final porosity of 53 vol.% and 75 vol.% with pore sizes between 180 and 250 µm. Cr_2AlC ceramics with closed porosity can only be obtained by applying pressure during the sintering process. Therefore, Field-Assisted Sintering Technology/Spark Plasma Sintering (FAST/SPS) was used to sinter Cr_2AlC ceramics to a high density. The sintering conditions in this case were heating rate of 100 K/min, maximal temperature of 1473 K, dwell time of 10 min, and uniaxial pressure of 50 MPa. The sintered ceramics present a closed porosity of 2.0 vol. %, and similar particle size than the porous ceramics consolidated by pressureless sintering. In summary, three Cr_2AlC ceramics were produced containing different porosity: 2, 53, and 75 vol.%. Hence, hereafter these ceramics are labelled as 2%, 53% and 75%, respectively. The microstructures of the prepared ceramics in detail are reported in the previous study [17].

The large ceramics were then cut into specimens of cylindrical shapes with a diameter of 6.0 to 6.5 mm and a height of 9 mm for creep testing by using electrical discharge machining. The details of the setup that has been used for creep testing have been explained in the previous studies [24][25]. The creep tests were carried out in Ar from 1073 K to 1173 K (maximum temperature limited by the experimental setup) and in air from 1073 K to 1473 K under the application of a uniaxial compressive load. A compressive prestress being smaller than 0.1 MPa was applied during heating to keep the specimen fixed. Stresses of 1 to 12 MPa were applied to determine the creep rates, where maximum and minimum applied stresses were determined depending on deformation at each temperature. Each creep measurement was terminated when steady-state deformation was confirmed and continued until an integral deformation reached to ~100 µm. Each sample was examined first at 1073 K to 1173 K in Ar (with 4.5% of H_2), and then at 1073 K to 1473 K in air during heating, followed by subsequent tests at 1473 K to 1273 K in air during cooling.

(Note that, for the test in Ar, the chamber was first vacuumed down to the pressure of ~10^{-2} mbar and

cleansed by the gas with the pressure of ~300 mbar. After repeating this process twice, the chamber was filled up with the gas again up to the pressure of 1013 mbar, and the pressure in the chamber was maintained between 1000 – 1090 mbar during the whole tests by adding and releasing the gas.) The same specimen was examined in the above tests, which means one specimen was tested under multiple thermal and mechanical-loading cycles at different temperatures in different atmospheres, whilst additional tests were performed using another specimen under selected conditions to confirm the obtained results.

The minimum creep strain rate in the secondary stage (simply called "creep rate" hereafter) is known to depend on temperature T and stress σ, and can be expressed by the following equation [26]:

$$\dot{\varepsilon}_{\min} = \dot{\varepsilon}_0 A \left(\frac{\sigma}{\sigma_0} \right)^n \exp\left(-\frac{Q}{RT} \right) \quad (1),$$

where A, n, Q, and R are a stress-independent constant (Dorn constant), stress exponent, activation energy for creep, and gas constant, respectively.

Some edges of the ceramics after the creep tests (but not fractured) were mirror-polished with SiC sandpaper, diamond pastes (3 and 1 μm), and colloidal silica (~80 nm) using a polishing machine (IM-P2, IMT). The polished surfaces were visualized by using a back-scattered electron microscope (BSEM) (SU1510, Hitachi High-Technologies). Energy dispersive X-ray analysis (EDX) (XFlash 4010, Bruker) was also performed for chemical composition analysis.

3. Results

Figure 1 shows typical histories of the creep deformation (porous sample 53% as an example). The sample shows a larger creep deformation at higher temperature or under higher stress; however, different creep deformations during the heating and cooling are observed despite the same temperature and stress conditions (1273 K and 10 MPa in Fig. 1). The creep rate was determined from the slope in the secondary stage simply using a linear fitting and the results are summarised in Figs. 2 and 3.

Figure 2 shows the Arrhenius plot of the creep rate of the ceramics 2, 53, and 75% measured in the temperature range of 1073 K and 1473 K in Ar and air under the compressive stress of 1 to 12 MPa. The

sample 53% was investigated in detail, whilst the other ceramics 2% and 75% were examined only under selected conditions so as to determine the creep parameters. It should be noted that the creep rate lower than 10^{-8} s^{-1} will be strongly affected by experimental uncertainties, i.e. drift and noise. Also, the present test even in Ar seems to have oxidised ceramics more or less, as the colour of the ceramics tested in Ar turned to slightly black from metallic silver. The creep rates measured during heating under constant stress show as to be expected a monotonic increase with increasing temperature, whilst the rates measured during cooling show a monotonic decrease with decreasing temperature. However, unexpectedly the creep rates of the ceramics 53% and 75% during cooling are much lower than the ones during heating if compared under the same conditions.

Figure 3 shows the creep rates as a function of applied stress of the ceramucs 2%, 53%, and 75%. As might be expected, the creep rates measured at a particular temperature increase with increasing stress, and the slopes are similar to each other regardless of temperature. Again as might be expected, the porous 75% exhibits much higher creep rates than 53%. The creep rates measured during cooling are much lower than those during heating similar as seen in 53%, whereas there is no difference between the creep rates between heating and cooling for the dense 2%.

Figure 4 presents a regression analysis of the creep rates of the ceramics 2, 53, and 75%, which were obtained using Eq. (1) with $\varepsilon_0 = 1$ s^{-1} and $\sigma_0 = 1$ MPa [23]. The determined creep parameters Q, n, and A are summarised in Table 1. The dense ceramics 2% yields only one regression line regardless of heating or cooling, whereas the creep rates of porous ceramics 53% and 75% measured during cooling are much lower than those during heating.

Figure 5 shows a BSEM image and EDX element mapping of the porous sample 53% after the creep tests. There are two layers with ~ 3 to 8 μm thick grown on the matrix Cr_2AlC phase; the outer layer appears darker whereas the inner one is lighter in Fig. 5(a). The outer and inner scales are rich in Al and Cr, respectively, as revealed in Fig. 5(b). Figure 6 (a) and (b) shows a BSEM image and EDX element mapping of sample 75% after the creep tests with lower magnification. The same layers are confirmed to form all over the surface of the porous structure including pores. In addition, the pores that existed on the surface were closed after the creep tests due to the formation of the scales, and the apparent micro-cracks propagating inwards the sample were also closed by those scales.

4. Discussion

Oxide and carbide scale growth on the surface of the matrix Cr_2AlC phase (within the pores) were confirmed after the creep tests, as shown in Figs. 5 and 6, which can be assigned to be α-Al_2O_3 and Cr_7C_3, respectively, in agreement with literature reports [17][27]. It should be noted that these scales formed gradually but surely during the creep tests during heating whilst the specimens were exposed to the temperatures ranging from 1073 K to 1473 K for many hours including the holding period (~ 1 h) before each test. As these scales on Cr_2AlC are known to grow rapidly at higher temperature, especially within the first few hours [3][27], most of the scales observed after the test probably formed during the creep test at the highest exposure temperature, 1473 K. Thus, the obtained results inevitably include the oxidation effect: the creep rates measured during heating are of non-oxidised or being-oxidised ceramics in the present case, whereas the creep rates measured during cooling are of the ceramics after the oxidation.

4.1. Creep mechanism of dense Cr_2AlC

First, we discuss the creep mechanism of dense Cr_2AlC (with 2% porosity), which is considered to be less influenced by the oxidation, as the relative volume of the oxidation layers is small compared to the whole specimen volume [26]. The dense Cr_2AlC possesses a consistent creep rate during heating and cooling at a particular temperature and stress condition, as shown in Fig. 2(a), which suggests that the same thermally-activated, rate-controlling process has to be operative within the entire temperature range. The obtained creep parameters Q and n summarized in Table 1 are similar to the ones of dense Ti_3SiC_2 obtained under tension and compression at lower temperature and/or stress [26,28,29]; for example, the parameters Q and n of fine-grain Ti_3SiC_2 are 445-537 kJ/mol and 1.5–1.9, respectively. The mechanism aiding the secondary creep of Ti_3SiC_2 has been attributed mainly to dislocation creep, since a weak dependence of the creep rate on the grain size was observed. The creep behaviour of dense Ti_2AlC has also been presented in the literature [30]: the parameters Q and n of Ti_2AlC were 362 kJ/mol and 2.5, respectively, and the observation of the fracture surface indicated that dislocation creep with possibly grain boundary sliding was the dominant creep mechanism. The creep mechanism of Ti_3AlC_2 has been also studied recently [31]: the parameter n was 2.34–2.50, and based on TEM observations it was concluded that creep deformation was governed by grain boundary sliding, either through dislocation or diffusion. (Note that most of these investigations still suggest a necessity for further investigations to clarify the creep mechanism.)

The creep parameters of Cr_2AlC, obtained for the first time in the current study, are overall comparative with those above results on the other MAX phases; thus, the creep behaviour of dense Cr_2AlC may be governed by the dislocation motion and/or the grain boundary sliding. However, it can be presumed from Figs. 5 and 6 and also various oxidation tests in the literature [3][27] that fresh surfaces possibly that formed by grain boundary sliding are immediately oxidized at elevated temperatures, which possibly hinders continuous creep deformation. Furthermore, since the oxidation rate depends significantly on temperature, a creep deformation by grain boundary sliding cannot to be expressed by a single thermally-activated process in the wide temperature range studied in the current work. There was also no obvious sign of grain boundary sliding observed at the surfaces and the polished cross-section. Therefore, it appears to be reasonable to consider that the dominant creep mechanism of Cr_2AlC is dislocation motion as observed for Ti_3SiC_2, which still needs further verification.

4.2. Creep mechanism of porous Cr_2AlC

It has been suggested that the creep rate of open-cell foams with porosity p can be predicted by the following equation using creep parameters Q and n of dense material [32]:

$$\dot{\varepsilon}_{\min} = \dot{\varepsilon}_0 AB\left(\frac{\sigma}{\sigma_0}\right)^n \exp\left(-\frac{Q}{RT}\right) \quad (2)$$

where

$$B = \frac{0.6}{n+2}\left(\frac{1.7(2n+1)}{n}\right)^n (1-p)^{\frac{-(3n+1)}{2}} \quad ,$$

which implies that the thermally-activated process, expressed mathematically by the term Q, is the same for dense and porous ceramics. For example, similar activation energies were observed for dense and porous zirconia [33]. In the present case, however, the activation energies Q of the porous ceramics are lower than the one of the dense one during heating but slightly higher during cooling, whilst the stress exponent n is within the range 1.9 to 4.7. The creep rate obtained during the heating was considered to be affected by the in-situ oxidation. For further discussion, the creep rate of non-oxidised porous Cr_2AlC 53% was estimated as follows.

The oxidation of Cr_2AlC has been investigated in the previous studies [17,27]. Lin et al. [27] performed

a thermogravimetric analysis on Cr_2AlC and found that the oxidation kinetics follows the parabolic rate law, $(\Delta W/A) = k_p t$, where $\Delta W/A$ is the mass gain per unit area and t is time. The parabolic oxidation rate constant k_p follows the Arrhenius law, $k_p = k_0 \exp(-Q/RT)$, with the activation energy Q = 298 kJ/mol. Gonzalez et al. [17] examined the oxidation of porous Cr_2AlC by thermogravimetric analysis, and the observed oxidation behaviour at 1573 K appears to be comparable to the above result [27] in terms of $\Delta W/A$. On the basis of these studies, the mass gain per unit area $\Delta W/A$ of the present porous Cr_2AlC 53% in the present experiment was estimated using the actual dwell times at each temperature.

Figure 7(a) shows the relationship between the estimated oxidation level ($\Delta W/A$) and the creep rate of the ceramic 53% under 10 MPa, as an example. Note that, in addition to the results shown in Figs. 1 to 4, the results of the porous 53% pre-oxidised at 1473 K for 1 h were tested at 1073 K to 1473 K under 10 MPa and included in Fig. 7(a). The creep rate is reduced as the oxidation level increases, and the oxidation effect on the creep rate is more significant at lower temperature. The creep rate of "non-oxidised" ceramics 53% (i.e., $\Delta W/A = 0$) was then estimated by extrapolation. Figure 7(b) presents a regression analysis of the creep rates of the non-oxidised ceramics 53%. The determined creep parameters Q, n, and A of non-oxidised porous Cr_2AlC 53% are 221 (± 4) kJ/mol, 1.6 (± 0.2), and 26, respectively, which are similar to the parameters during the heating. This suggests that the change in the parameters between heating and cooling for porous Cr2AlC could be mainly attributed to the oxidation at 1473 K. (Note that additional creep tests with porosity 75% performed at 1173 K under 5 MPa oxidised at (1173 K,) 1273 K, 1373 K, and 1473 K for ~1 h demonstrated that the creep rate was only reduced approximately by half after heating up to 1373 K (from 1.7×10^{-7} to 6.6×10^{-8}), whereas it was decreased by two orders of magnitude after heating 1474 K (1.1×10^{-5}), which also suggested that the oxidation at 1473 K is dominant.)

Although the apparent activation energy of porous Cr_2AlC during heating and the estimated activation energy of the non-oxidised porous Cr_2AlC are relatively lower than that of the dense Cr_2AlC but slightly higher during heating (or after oxidation), the stress exponents are roughly comparable each other and also to the literature [*], which probably indicates that the same creep mechanism, i.e., possibly the dislocation creep as discussed above, is essentially dominant for the dense and porous Cr_2AlC ceramics.

4.3. Improvement in creep resistance of porous Cr_2AlC

The creep rates of the porous ceramics were significantly lower during cooling, i.e., after oxidation, than those during the heating or before oxidation. The significant improvement in the creep behaviour of the porous ceramics after oxidation can be attributed to the formation of the scales, as observed for other porous alloys [34]. The possible contribution of the formed scales to the improvement of the creep resistance could be two factors: reduced deformation rate due to enhanced creep resistance by the aluminium oxide scale and self-healing.

It is known that the mechanical strength of dense Cr_2AlC suddenly decreases above 873–1073 K [35,36] and the brittle-ductile transition temperature is estimated to be 1073–1173 K [36]. The current tests confirmed that the dense sample exhibits linear elastic behaviour at room temperature but the one almost without oxidation exhibits not elastic but plastic response above 1073 K, even for a compressive stress of only a few MPa. On the other hand, aluminium oxide with high purity is known to maintain its excellent mechanical stability up to 1473 K [37]. Therefore, the formation of the scales, especially aluminium oxide, on Cr_2AlC could decrease the apparent deformation of the porous ceramics, which probably results in the improvement of its creep resistance. The volume expansion due to the formation of the scales also could partially contribute to the increase of the apparent creep resistance.

However, the effect of the scale formation might not only lead to an apparent creep resistance enhancement, but also to a healing of cracks and defects, as reported in the literature [38][39]: for instance, a crack with a length of 10 μm in Cr_2AlC can be healed (or closed) at 1473 K within 12 h by the formation of the aluminium oxide scale, which however mechanically is the same effect as verified for small pores by the same picture. Also, our observation shown in Figs. 5 and 6 clearly confirms the self-healing of micro-cracks and surface defects. Although the self-healing effect appears to partially aid to the improvement of the creep resistance, the dominant improvement factor can still be assumed to be the apparent creep resistance enhancement effect by the thoroughly-formed aluminium oxide layer, since the loading mode was compressive (not tensile to open those cracks) and also the number of the observed micro-cracks was low. In addition, for micro-cracks a more non-linear behaviour, if they continue to grow, might be expected, although final conclusions will require further tests with and without peroxidation and cooling down after different exposure times.

4.4. Comparison with other refractory materials

Figure 8 compares the creep rates of 2%, 53%, and 75% under 1 MPa and 3 MPa of compressive stress, which are estimated using the creep parameters shown in Table 1. The estimated creep rate of non-oxidised 53% and also the creep rate of dense Ti_3SiC_2 [26] are also shown for comparison in Fig. 8. For non-oxidised or being-oxidised ceramics, the creep rate is generally higher for a higher porosity at lower temperature, whereas the oxidised porous ceramics show a comparable or even lower creep rate than the oxidised rather dense sample (porosity 2%), which could be attributed to the formed scales on the outer and inner surfaces of the porous structures.

Figure 9 compares the creep rates of the porous Cr_2AlC 75% (in-situ oxidised and non-oxidised) with the creep rates of various porous refractory materials such as high-temperature alloys and conventional ceramics [33, 40-43]. Although a direct comparison is difficult as they have different porosities and were examined under different conditions, Fig. 9 clearly demonstrates that the oxidised porous Cr_2AlC has a comparative ability to withstand creep deformation as the other porous materials and has a high potential as a refractory material especially considering its machinability and light-weight. The results indicate that pre-oxidation of porous Cr_2AlC before application can be effective and, furthermore, the creep-resistance will be naturally but significantly improved during high-temperature application.

5. Conclusions

The creep behaviours of the dense and porous Cr_2AlC ceramics were investigated in this study. The porosities of examined sample were 1.9% (dense), 53% (porous) and 75% (porous). The creep tests were performed mostly in air from 1073 K to 1473 K upon heating and then from 1473 K to 1073 K upon cooling.

The EDX analysis confirmed that the aluminium oxide (Al_2O_3) and carbide (Cr_7C_3) scales grown on the dense and porous Cr_2AlC phase after the creep tests with the thickness of 3 to 8 μm. The creep rate of the porous Cr_2AlC measured during cooling was significantly lower than the one during heating due to the oxide and carbide scales formed during the creep tests at the high temperature 1473 K, whilst the dense Cr_2AlC has the consistent creep rate during heating and cooling: For example, the creep rate of the porous 53% under 5 MPa at 1273 K was 2.2×10^{-7} during heating and 5.0×10^{-9} during cooling. The scales seamlessly formed on the whole surface of pores probably worked to increase the stiffness and also heal

defects and micro-cracks, which improved the creep resistance of the porous ceramics. The creep rate of the being-oxidised Cr_2AlC ceramics during heating is generally higher for higher porosity at higher temperature under higher stress, whereas the oxidised porous Cr_2AlC could be more creep-resistance than the dense one under certain conditions, due to the reinforcement by the scales. The regression analysis demonstrated that the porous Cr_2AlC showed relatively lower activation energies (219–242 kJ/mol) than the dense Cr_2AlC (429 kJ/mol) during heating but slightly higher values (502–506 kJ/mol) during cooling, although these activation energies and the stress exponents (1.7–4.8) for creep deformation were roughly comparable each other and also to the other MAX phase ceramics, which probably indicated the common creep mechanism attributed to dislocation motion. The comparison with other porous high-temperature alloys and conventional ceramics revealed that the oxidised porous Cr_2AlC has a high potential as a refractory material especially considering its machinability and light-weight.

ACKNOWLEDGEMENTS

This work is partially supported by JSPS KAKENHI Grant Number 15KK0229. Jesus Gonzalez-Julian thanks the financial support by the Germany´s Federal Ministry of Education and Research (“Bundesministerium für Bildung und Forschung”) under the MAXCOM project (03SF0534).

REFERENCES

[1] M.W. Barsoum, MAX Phases. Properties of Machinable Ternary Carbides and Nitrides, Wiley VCH, 2013.

[2] B.M. Radovic, M.W. Barsoum, MAX phases : Bridging the gap between metals and ceramics, Am. Ceram. Soc. Bull. 92 (2013) 20–27.

[3] D.J. Tallman, B. Anasori, M.W. Barsoum, A critical review of the oxidation of Ti_2AlC, Ti_3AlC_2 and Cr_2AlC in Air, Mater. Res. Lett. 1 (2013) 115–125. doi:10.1080/21663831.2013.806364.

[4] J.L. Smialek, Oxygen diffusivity in alumina scales grown on Al-MAX phases, Corros. Sci. 91 (2015) 281–286. doi:10.1016/j.corsci.2014.11.030.

[5] A.S. Farle, C. Kwakernaak, S. van der Zwaag, W.G. Sloof, A conceptual study into the potential of Mn+1AXn-phase ceramics for self-healing of crack damage, J. Eur. Ceram. Soc. 35 (2015) 37–45. doi:10.1016/j.jeurceramsoc.2014.08.046.

[6] J. Gonzalez-Julian, T. Go, D.E. Mack, R. Vaßen, Environmental resistance of Cr_2AlC MAX phase under thermal gradient loading using a burner rig, J. Am. Ceram. Soc. 101 (2018) 1841–1846.

[7] J.L. Smialek, Environmental resistance of a Ti_2AlC-type MAX phase in a high pressure burner rig, J. Eur. Ceram. Soc. 37 (2017) 23–34. doi:10.1016/j.jeurceramsoc.2016.07.038.

[8] M.W. Barsoum, M. Radovic, Elastic and Mechanical Properties of the MAX Phases, Annu. Rev. Mater. Res. 41 (2011) 195–227. doi:10.1146/annurev-matsci-062910-100448.

[9] P. Eklund, M. Beckers, U. Jansson, H. Högberg, L. Hultman, The $M_{n+1}AX_n$ phases: Materials science and thin-film processing, Thin Solid Films. 518 (2010) 1851–1878. doi:10.1016/j.tsf.2009.07.184.

[10] J. Gonzalez-Julian, J. Llorente, M. Bram, M. Belmonte, O. Guillon, Novel Cr_2AlC MAX-phase/SiC fiber composites: Synthesis, processing and tribological response, J. Eur. Ceram. Soc. 37 (2017). doi:10.1016/j.jeurceramsoc.2016.09.029.

[11] Z. Zhang, S.H. Lim, J. Chai, D.M.Y. Lai, P.C. Lim, A.K.H. Cheong, S. Wang, H. Jin, J. Pan, Kerosene-fuelled high velocity oxy-fuel (HVOF) spray of Ti2AlC MAX phase powders, J. Alloys Compd. 735 (2018) 377–385. doi:10.1016/j.jallcom.2017.11.157.

[12] Z. Sun, A. Murugaiah, T. Zhen, A. Zhou, M. Barsoum, Microstructure and mechanical properties of porous Ti3SiC2, Acta Mater. 53 (2005) 4359–4366. doi:10.1016/j.actamat.2005.05.034.

[13] A.R. Studart, U.T. Gonzenbach, E. Tervoort, L.J. Gauckler, Processing routes to macroporous ceramics: A review, J. Am. Ceram. Soc. 89 (2006) 1771–1789. doi:10.1111/j.1551-2916.2006.01044.x.

[14] L. Hu, R. Benitez, S. Basu, I. Karaman, M. Radovic, Processing and characterization of porous Ti_2AlC with controlled porosity and pore size, Acta Mater. 60 (2012) 6266–6277. doi:10.1016/j.actamat.2012.07.052.

[15] B. Velasco, E. Gordo, L. Hu, M. Radovic, S.A. Tsipas, Influence of porosity on elastic properties of Ti2AlC and Ti3SiC2MAX phase foams, J. Alloys Compd. 764 (2018) 24–35. doi:10.1016/j.jallcom.2018.06.027.

[16] B. Velasco, E. Gordo, S.A. Tsipas, MAX phase Ti2AlC foams using a leachable space-holder material, J. Alloys Compd. 646 (2015) 1036–1042. doi:10.1016/j.jallcom.2015.05.235.

[17] J. Gonzalez-Julian, S. Onrubia, M. Bram, C. Broeckmann, R. Vaßen, O. Guillon, High temperature oxidation and compressive strength of Cr2AlC MAX phase foams with controlled porosity, J. Am.

Ceram. Soc. 101 (2017) 542-552.

[18] C.R. Bowen, T. Thomas, Macro-porous Ti2AlC MAX-phase ceramics by the foam replication method, Ceram. Int. 41 (2015) 12178–12185. doi:10.1016/j.ceramint.2015.06.038.

[19] Z. Sun, Y. Liang, M. Li, Y. Zhou, Preparation of reticulated MAX-phase support with morphology-controllable nanostructured ceria coating for gas exhaust catalyst devices, J. Am. Ceram. Soc. 93 (2010) 2591–2597. doi:10.1111/j.1551-2916.2010.03776.x.

[20] S. Karimi, T. Go, R. Vaßen, J. González-Julián, Cr_2AlC MAX phase foams by replica method, J. Am. Ceram. Soc. (2019) Submitted.

[21] M. Potoczek, E. Guzi de Moraes, P. Colombo, Ti_2AlC foams produced by gel-casting, J. Eur. Ceram. Soc. 35 (2015) 2445–2452. doi:10.1016/j.jeurceramsoc.2015.03.015.

[22] T. Fey, M. Stumpf, A. Chmielarz, P. Colombo, P. Greil, M. Potoczek, Microstructure, thermal conductivity and simulation of elastic modulus of MAX-phase (Ti_2AlC) gel-cast foams, J. Eur. Ceram. Soc. 38 (2018) 3424–3432. doi:10.1016/j.jeurceramsoc.2018.04.012.

[23] J. Gonzalez-Julian, S. Onrubia, M. Bram, O. Guillon, Effect of sintering method on the microstructure of pure Cr_2AlC MAX phase ceramics, J. Ceram. Soc. Japan. 124 (2016) 415–420. doi:10.2109/jcersj2.15263.

[24] B. Rutkowski, J. Malzbender, T. Beck, R.W. Steinbrech, L. Singheiser, Creep behaviour of tubular $Ba_{0.5}Sr_{0.5}Co_{0.8}Fe_{0.2}O_{3-\delta}$ gas separation membranes, J. Eur. Ceram. Soc. 31 (2011) 493–499. doi:10.1016/J.JEURCERAMSOC.2010.10.030.

[25] Y. Zou, F. Schulze-Küppers, J. Malzbender, Creep behavior of porous $La_{0.6}Sr_{0.4}Co_{0.2}Fe_{0.8}O_{3-\delta}$ oxygen transport membrane supports, Ceram. Int. 41 (2015) 4064–4069. doi:10.1016/J.CERAMINT.2014.11.100.

[26] M. Radovic, M.W. Barsoum, T. El-Raghy, S.M. Wiederhorn, Tensile creep of coarse-grained Ti_3SiC_2 in the 1000–1200°C temperature range, J. Alloys Compd. 361 (2003) 299–312. doi:10.1016/S0925-8388(03)00435-3.

[27] Z.J. Lin, M.S. Li, J.Y. Wang, Y.C. Zhou, High-temperature oxidation and hot corrosion of Cr_2AlC, Acta. Mater. 55 (2007) 6182-6191.

[28] M. Radovic, M.W. Barsoum, T. El-Raghy, S.Wiederhorn, Tensile creep of fine grained (3–5 mm) Ti_3SiC_2

in the 1000–1200°C temperature range, Acta Mater. 49 (2001) 4103-4112.

[29] T. Zhen, M.W. Barsoum, S.R. Kalidindi, M. Radovic, Z.M. Sun, T. El-Raghy, Compressive creep of fine and coarse-grained T_3SiC_2 in air in the 1100–1300°C temperature range, 53 (2005) 4963-4973.

[30] D.J. Tallman, M. Naguib, B. Anasori, M.W. Barsoum, Tensile creep of Ti_2AlC in air in the temperature range 1000–1150°C, Scripta Mater. 66 (2012) 805-808.

[31] E. Drouelle, A. Joulain, J. Cormier, V. Gauthier-Brunet, P. Villechaise, S. Dubois, P. Sallot, Deformation mechanisms during high temperature tensile creep of Ti_3AlC_2 MAX phase, J. Alloys Compd. 693 (2017) 622-630.

[32] E.W. Andrews, L.J. Gibson, M.F. Ashby, The creep of cellular solids, Acta Mater. 47 (1999) 2853-2863.

[33] F. Cabannes, K. Dembinski, Y. Bigay, Creep behavior of zirconia foams used in electrical furnaces (2100 K - air), Journal de Physique 47 (1986) C1-649-654

[34] J.A. Scott, D.C. Dunand, Processing and mechanical properties of porous Fe-26Cr-1Mo for solid oxide fuel cell interconnects 58 (2010) 6125-6133.

[35] W. Tian, Z. Sun, H. Hashimoto, Y. Du, Compressive deformation behavior of ternary compound Cr_2AlC, J. Mater. Sci. 44 (2009) 102-107.

[36] W. TIan, Z. Sun, Y. Du, H. Hashimoto, Mechanical properties of pulse discharge sintered Cr_2AlC at 25–1000°C, Mater. Lett. 63 (2009) 670-672.

[37] R.G. Munro, Evaluated material properties for a sintered α-alumina, J. Am. Ceram. Soc. 80 (1997) 1919-1928.

[38] H.J. Yang, Y.T. Pei, J.Th.M. De Hosson, Oxide-scale growth on Cr_2AlC ceramic and its consequence for self-healing, Scripta Mater. 69 (2013) 203-206.

[39] R. Pei, S.A. McDonald, L. Shen, S. van der Zwaag, W.G. Sloof, P.J. Withers, P.M. Mummery, Crack healing behaviour of Cr_2AlC MAX phase studied by X-ray tomography, J. Eur. Ceram. Soc. 37 (2017) 441-450.

[40] J.A. Glasscock, L. Mikkelsen, Å.H. Persson, G. Pećanac, J. Malzbender, P. Blennow, F. Bozza, P.V. Hendriksen, Porous Fe21Cr7Al1Mo0.5Y metal supports for oxygen transport membranes: Thermo-mechanical properties, sintering and corrosion behavior, Solid State Ionics 242 (2013) 33-44.

[41] V.S. Bakunov, High-temperature creep in refractory ceramics. porous materials, Refractories 35 (1994) 317-321.

[42] A.M. Hodge, D.C. Dunand, Measurement and modeling of creep in open-cell NiAl foams, Metall. Mater. Trans. A 34A (2003) 2353-2363.

[43] K.S. Kim, J.Y. Yun, B.G. Choi, K.A. Lee, Effect of the pore size on the creep deformation behavior of Ni-Fe-Cr-Al porous metal, Met. Mater. Int. 20 (2014) 506-513.

Captions

Table 1 Parameters for high-temperature creep behaviour of dense and porous Cr_2AlC

Figure 1 Example of the creep deformation of porous Cr_2AlC (53%).

Figure 2 Arrhenius plots of creep rate of Cr_2AlC with the porosities of (a) 2%, (b) 53%, and (c) 75%.

Figure 3 Stress vs creep rate of Cr_2AlC with the porosities of (a) 2%, (b) 53%, and (c) 75%.

Figure 4 Regression analyses of creep rate of dense and porous Cr_2AlC with the porosities of (a) 2%, (b) 53%, and (c) 75%.

Figure 5 Polished cross-section of porous Cr_2AlC (53%) after the creep test in (a) BSEM image and (b) EDX element mapping, which show the oxide and carbide scales formed on the Cr_2AlC phase.

Figure 6 Polished cross-section of porous Cr_2AlC (75%) after the creep test in (a) BSEM image and (b) EDX element mapping, which show that the surface pores are closed by the scales and microcracks are healed by the scales.

Figure 7 Estimation of creep rate of “non-oxidised” porous Cr_2AlC (53%): (a) Oxidation level and creep rate and (b) regression analysis.

Figure 8 Estimation and comparison of the creep rates of dense and porous Cr_2AlC (2, 53, and 75%) under stress of (a) 1 MPa and (b) 3 MPa. “oxi” indicates the creep rate of the oxidised sample, i.e., the result

during cooling. The estimated creep rate of non-oxidised Cr_2AlC 53% and the creep rate of dense Ti_3SiC_2 are shown for comparison.

Figure 9 Comparison of the creep rates of in-situ oxidised and oxidised Cr_2AlC with refractory alloys and ceramics. Square symbol shows alloys, whilst circle shows ceramics. Open symbol shows highly porous ceramics (> 70%), whilst solid symbol shows relatively dense materials. Larger symbol indicates higher stress (> 20 MPa), whilst smaller symbols indicate lower stress.

Table 1 Parameters for high-temperature creep behaviour of dense and porous Cr_2AlC ceramics.

Porosity	Heating/Cooling	*Q*, kJ/mol	*n*	*A*
1.9%	Heating	429 ± 13	2.7 ± 0.2	2.3×10^{10}
	Cooling			
53%	Heating	242 ± 7	1.9 ± 0.1	65
	Cooling	506 ± 10	1.9 ± 0.1	1.4×10^{11}
75%	Heating	219 ± 10	1.7 ± 0.2	121
	Cooling	502 ± 38	4.8 ± 0.7	4.9×10^{11}

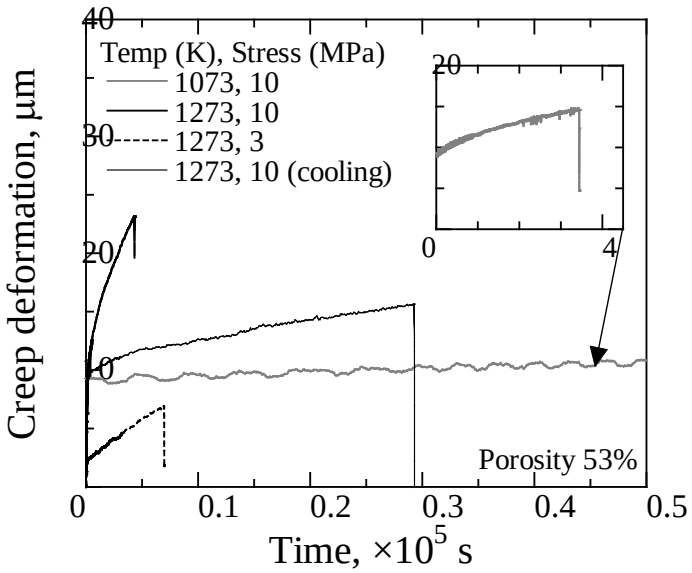

Figure 1 Example of the creep deformation of porous Cr_2AlC sample (53%).

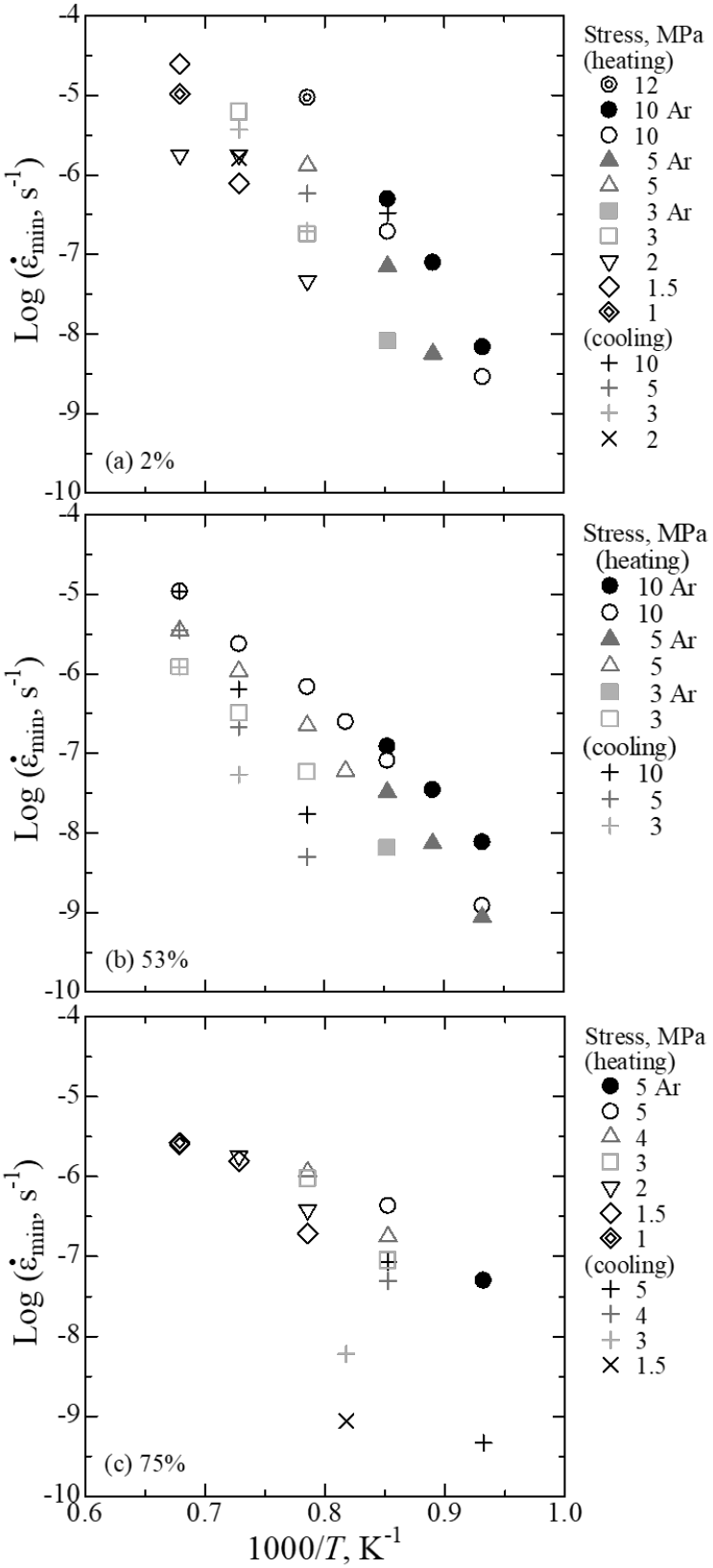

Figure 2 Arrhenius plots of minimum creep rate of Cr_2AlC ceramics with the porosities of (a) 2%, (b) 53%, and (c) 75%.

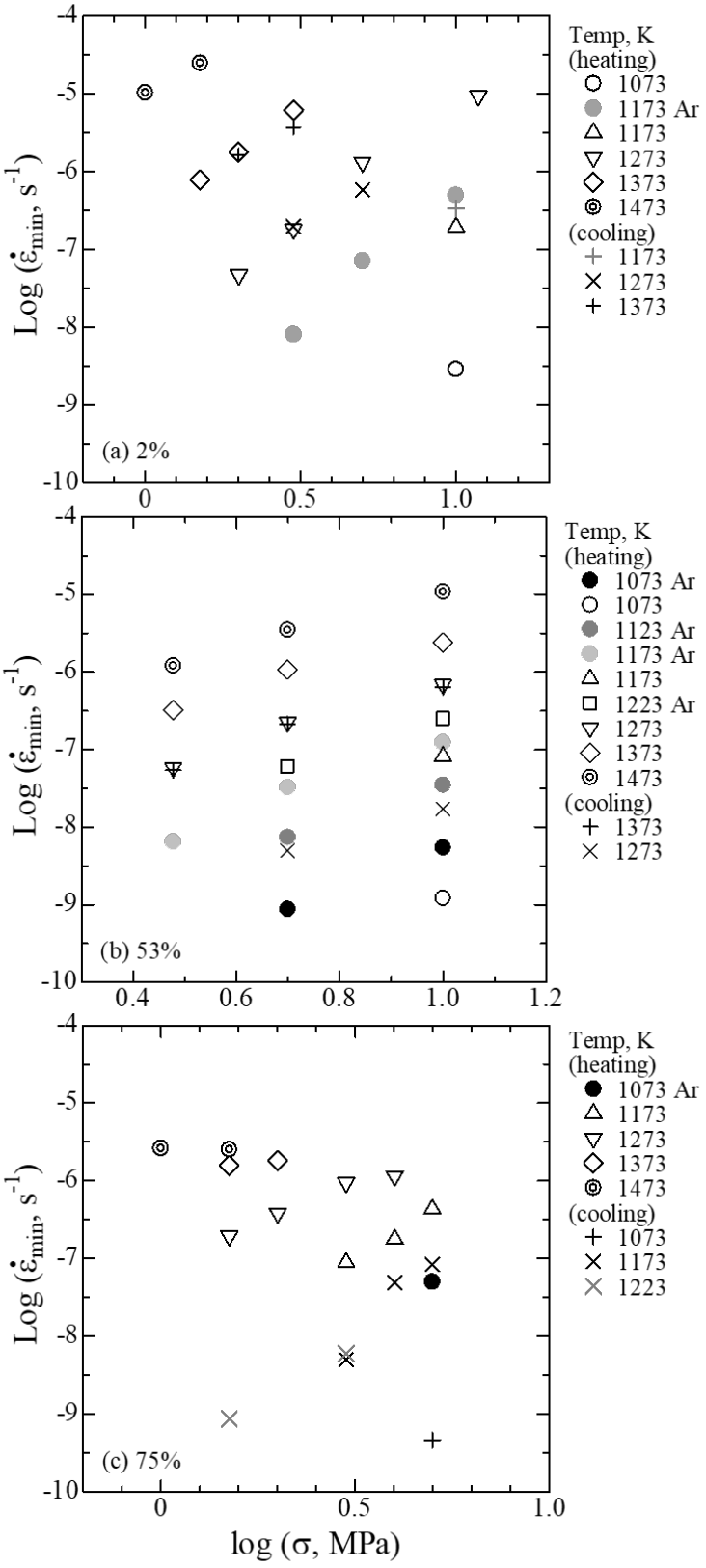

Figure 3 Stress vs minimum creep rate of Cr_2AlC ceramics with the porosities of (a) 2%, (b) 53%, and (c) 75%.

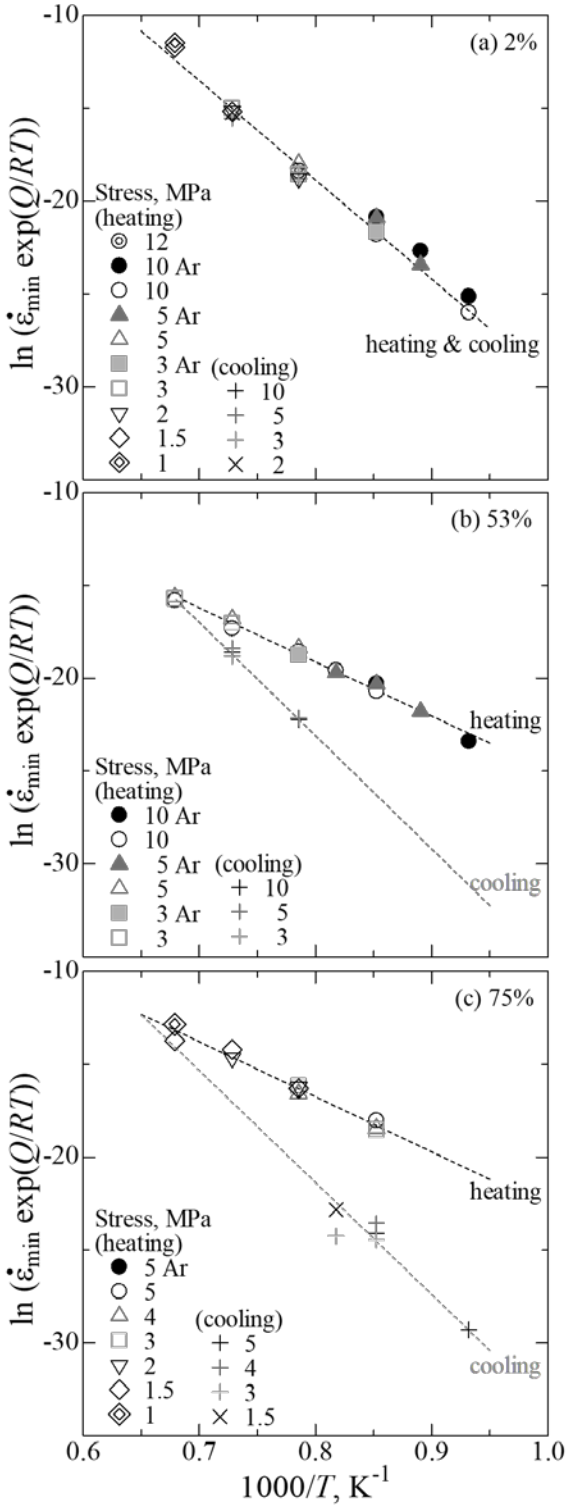

Figure 4 Regression analyses of creep rate of dense and porous Cr_2AlC ceramics with the porosities of (a) 2%, (b) 53%, and (c) 75%.

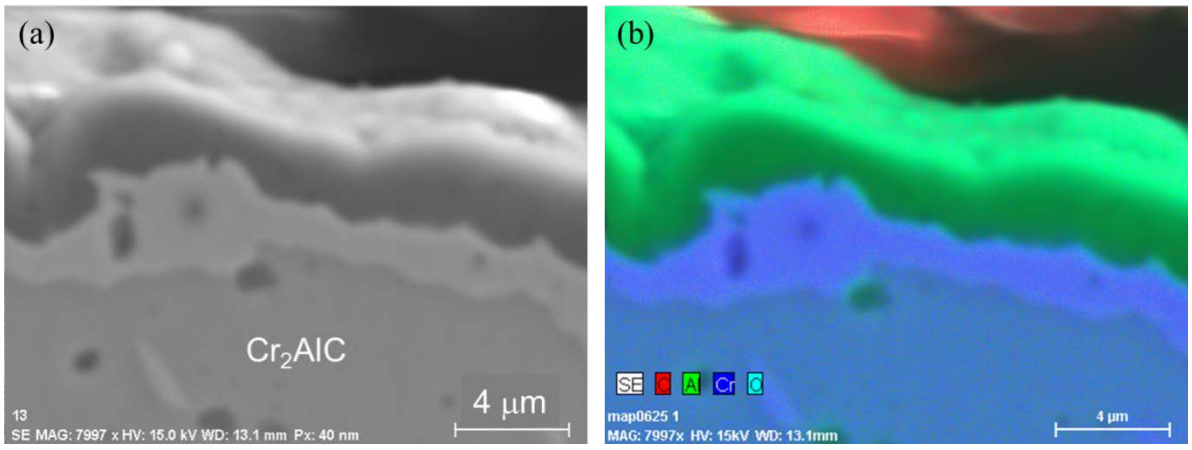

Figure 5 Polished cross-section of porous Cr_2AlC (53%) after the creep test in (a) BSEM image and (b) EDX element mapping, which show the oxide and carbide scales formed on the Cr_2AlC phase.

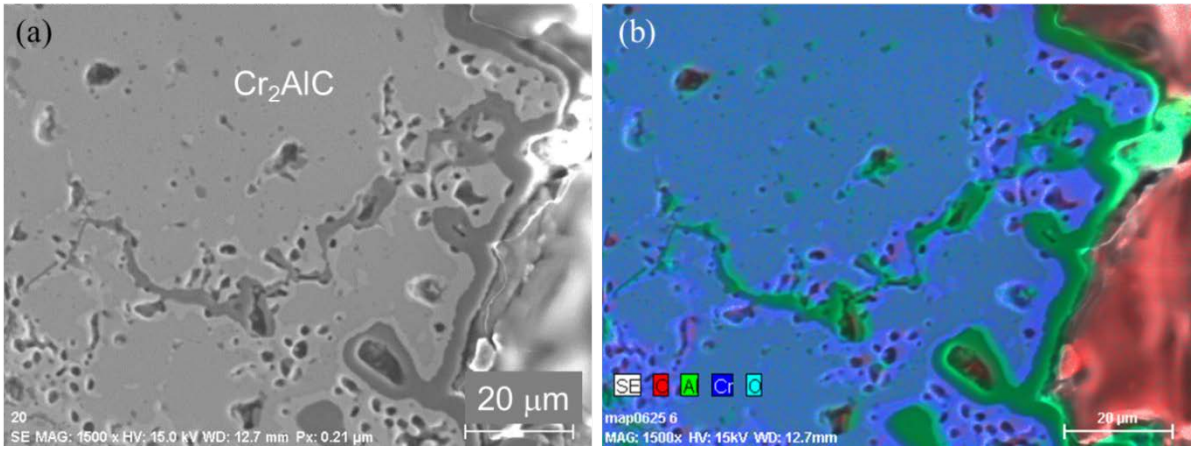

Figure 6 Polished cross-section of porous Cr_2AlC (75%) after the creep test in (a) BSEM image and (b) EDX element mapping, which show that the surface pores are closed by the scales and microcracks are healed by the scales.

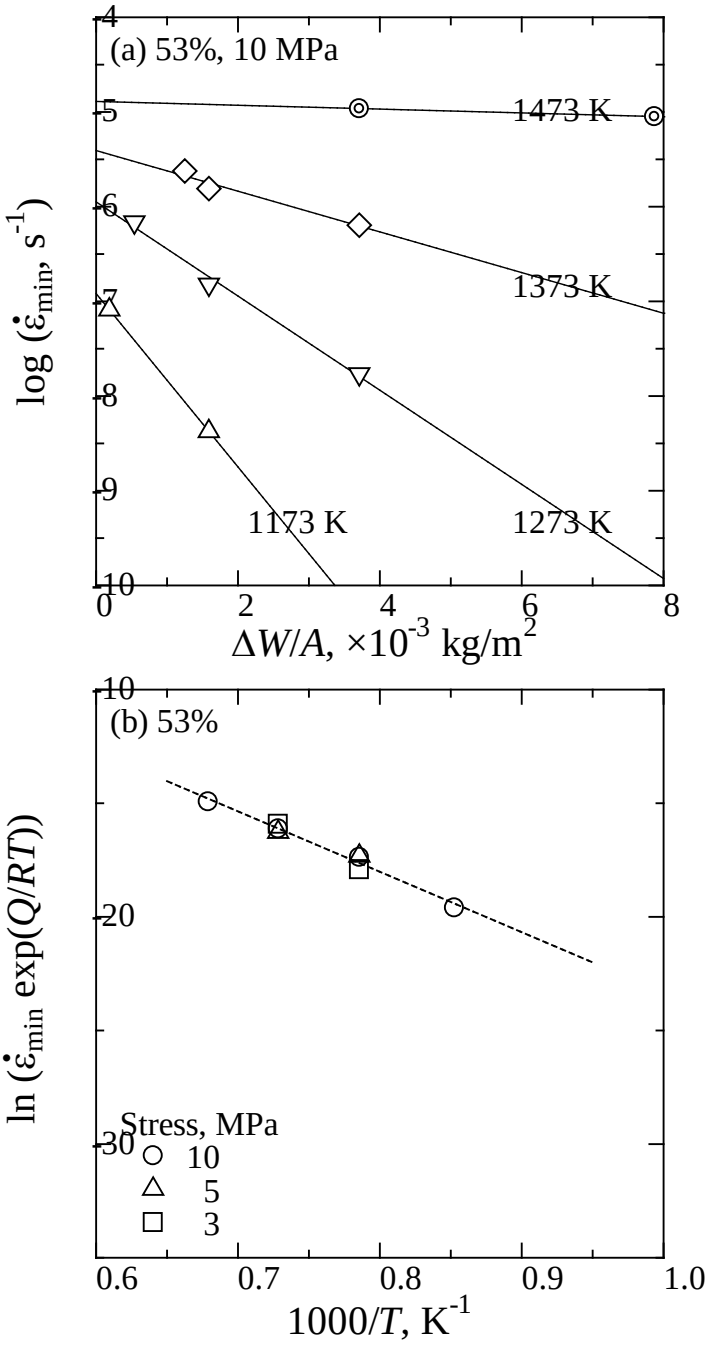

Figure 7 Estimation of creep rate of "non-oxidised" porous Cr_2AlC (53%): (a) Oxidation level and creep rate and (b) regression analysis.

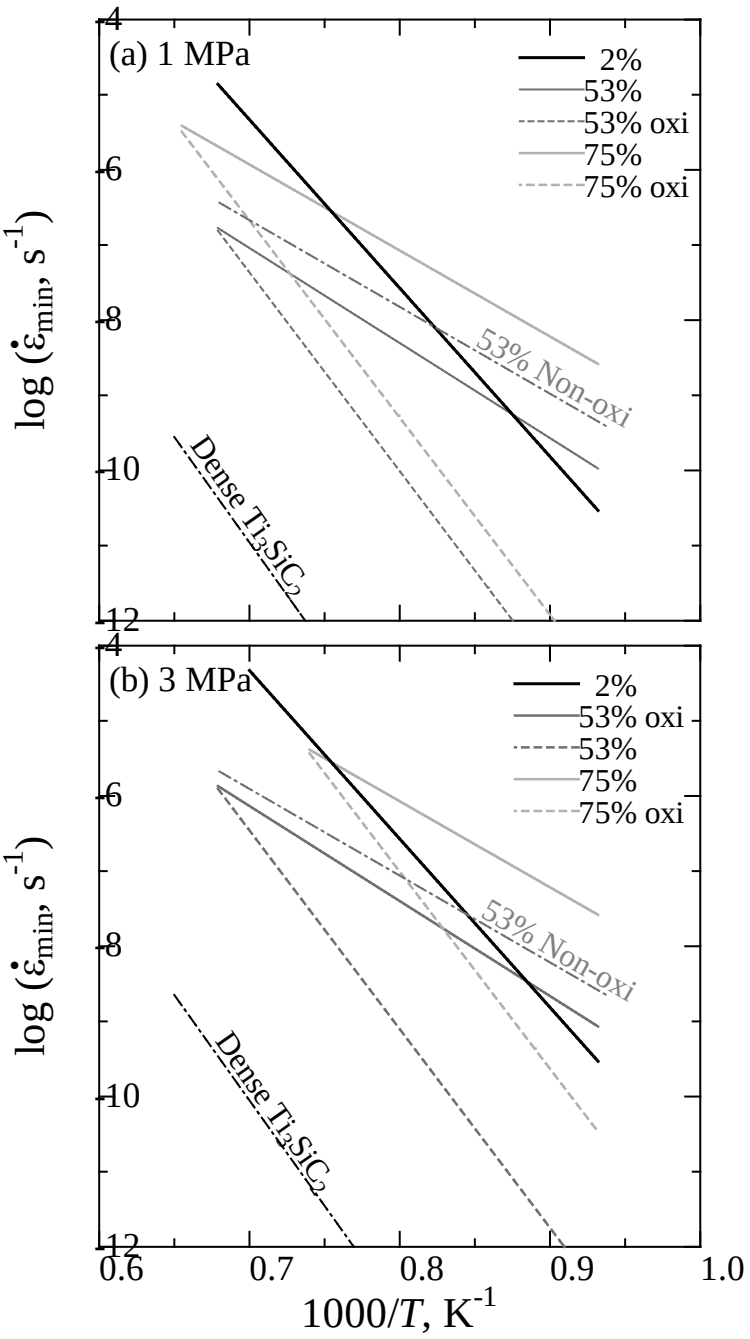

Figure 8 Estimation and comparison of the creep rates of dense and porous Cr_2AlC ceramics (2, 53, and 75%) under stress of (a) 1 MPa and (b) 3 MPa. “oxi” indicates the creep rate of the oxidised sample, i.e., the result during cooling. The creep rate of dense Ti3SiC2 is shown for comparison.

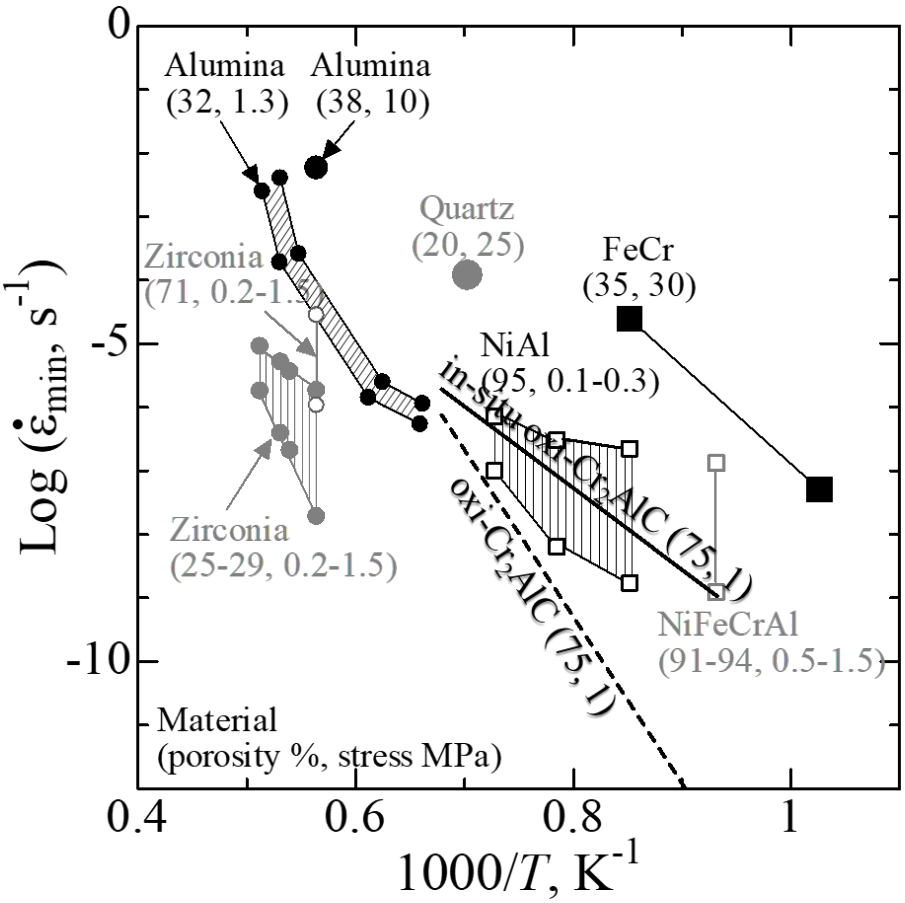

Figure 9 Comparison of the creep rates of non-oxidised and oxidised Cr_2AlC with refractory alloys and ceramics. Square symbol shows alloys, whilst circle shows ceramics. Open symbol shows highly porous ceramics (> 70%), whilst solid symbol shows relatively dense materials. Larger symbol indicates higher stress (> 20 MPa), whilst smaller symbols indicate lower stress.